

pubs.acs.org/synthbio Research Article

Yeast Intracellular Staining (yICS): Enabling High-Throughput, Quantitative Detection of Intracellular Proteins via Flow Cytometry for Pathway Engineering

Brett D. Hill, Ponnandy Prabhu, Syed M. Rizvi, and Fei Wen*



ACCESS I

Cite This: https://dx.doi.org/10.1021/acssynbio.0c00199

III Metrics & More

Cvtometrv



Article Recommendations

Yeast Intracellular Staining (yICS)

Cell Wall Removal

Antibody Staining

Pathway Engineering

Antibody Staining

Pathway Engineering

Antibody Staining

Pathway Engineering

Pathway Characterization

3 Plasmids

1 Plasmid

Pathway Engineering

Pathway Characterization

3 Plasmids

1 Plasmid

Pathway Engineering

ABSTRACT: The complexities of pathway engineering necessitate screening libraries to discover phenotypes of interest. However, this approach is challenging when desirable phenotypes cannot be directly linked to growth advantages or fluorescence. In these cases, the ability to rapidly quantify intracellular proteins in the pathway of interest is critical to expedite the clonal selection process. While Saccharomyces cerevisiae remains a common host for pathway engineering, current approaches for intracellular protein detection in yeast either have low throughput, can interfere with protein function, or lack the ability to detect multiple proteins simultaneously. To fill this need, we developed yeast intracellular staining (yICS) that enables fluorescent antibodies to access intracellular compartments of yeast cells while maintaining their cellular integrity for analysis by flow cytometry. Using the housekeeping proteins β actin and glyceraldehyde 3-phophate dehydrogenase (GAPDH) as targets for yICS, we demonstrated for the first time successful antibody-based flow cytometric detection of yeast intracellular proteins with no modification. Further, yICS characterization of a recombinant D-xylose assimilation pathway showed 3-plexed, quantitative detection of the xylose reductase (XR), xylitol dehydrogenase (XDH), and xylulokinase (XK) enzymes each fused with a small (6-10 amino acids) tag, revealing distinct enzyme expression profiles between plasmid-based and genome-integrated expression approaches. As a result of its highthroughput and quantitative capability, yICS enabled rapid screening of a library created from CRISPR-mediated XDH integration into the yeast δ site, identifying rare (1%) clones that led to an 8.4-fold increase in XDH activity. These results demonstrate the utility of yICS for greatly accelerating pathway engineering efforts, as well as any application where the high-throughput and quantitative detection of intracellular proteins is desired.

KEYWORDS: intracellular staining, flow cytometry, yeast, pathway engineering, xylose, CRISPR

A primary aim of synthetic biology is to engineer genetic networks to enhance or enable new cellular functions. Proteins play a fundamental role in these synthetic pathways and their manipulation is the focal point for the engineering of cellular systems. Due to an incomplete understanding of many protein structure—function relationships, as well as the complexity of systems-level protein—protein interactions inside the cell, it is often difficult to take a targeted, rational approach to pathway engineering. For these reasons, researchers often resort to generating libraries of gene overexpression, knockins, knockouts, or mutants followed by screening of these libraries to discover phenotypes of interest. To enable the rapid

screening of large libraries, desirable phenotypes are commonly linked to growth advantages or fluorescence; however, developing these linkages is rarely straightforward and thus may not be practical for many experimental systems.^{7,8} In these

Received: April 10, 2020 Published: June 30, 2020



s Supporting Information

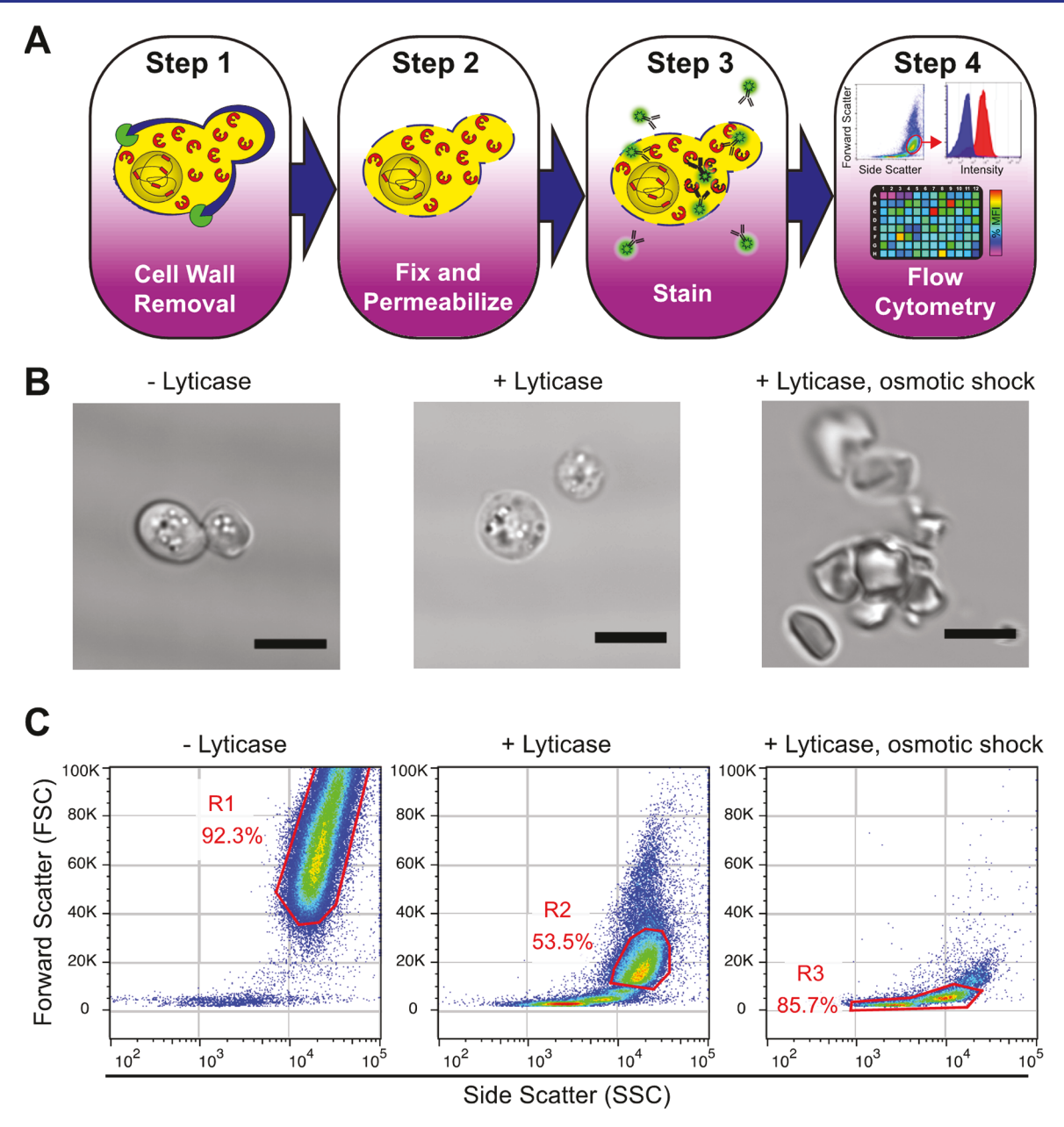


Figure 1. Design and feasibility of yeast intracellular staining (yICS). (A) Step 1 of the yICS procedure is the enzymatic removal of the cell wall to form spheroplasts, which are then fixed in Step 2 to provide structural integrity and permeabilized to enable antibody access to intracellular compartments. Antibody staining of intracellular POIs is performed in Step 3, followed by flow cytometry in Step 4. (B) Microscope images of cells before lyticase treatment (left), spheroplasts after lyticase treatment (middle), and lysed spheroplasts after osmotic shock in water (right). Scale bar is $5 \mu m$. (C) Flow cytometry is able to differentiate cells with intact cell walls (left, R1 gate), spheroplasts (middle, R2 gate), and lysed spheroplasts (right, R3 gate). The frequency of events in each gated population is shown adjacent to the gate.

cases, it is desirable to first reduce the library size by prescreening clones using indirect, but more obtainable indicators of cellular performance, such as protein expression. Because protein expression is the most engineered variable in synthetic biology, knowledge of protein expression levels can provide significant insights into a given clone's behavior. Therefore, high-throughput and quantitative protein detection methods that could facilitate the efficient screening of these libraries are of great interest.

Due to the ease of library generation and model-eukaryote status, *Saccharomyces cerevisiae* remains one of the most popular organisms for pathway engineering. ^{12–18} Further, its compatibility with flow cytometry allows for a convenient,

quantitative, and high-throughput means of protein detection as long as the protein expression can be coupled to fluorescence. While surface-displayed proteins can be conveniently labeled with fluorescent antibodies, ^{19–21} the vast majority of proteins that participate in cellular pathways are not surface accessible and therefore require alternative labeling strategies.²² The coupling of fluorescence to an intracellular protein of interest (POI) is most commonly accomplished by genetic fusion of the POI with a reporter protein.²³ The most ubiquitous reporter proteins are fluorescent proteins of which there is a diverse range that allow choice of spectra, pH stability, brightness, and photostability.²⁴ Other commonly used reporter proteins are "self-labeling" enzymes, such as the

Halo tag^{25,26} or SNAP/CLIP tag,^{27,28} that covalently bind to their externally added substrates. These substrates are usually conjugated with organic dyes, which offer superior photophysical properties compared to fluorescent proteins including greater brightness and broader spectral diversity.²⁹ However, both the fluorescent proteins and self-labeling enzymes are relatively large in size (20-33 kDa), and therefore their fusion with the POI often negatively affects protein function. 30-34 Moreover, the production of reporter protein fusions consumes additional cellular resources that can inhibit cell growth or detract from the production of pathway products. 35,36 Therefore, alternative methods for coupling fluorescence to POI expression that do not rely on large protein fusions are advantageous.

The tetracysteine-biarsenical system is one of the most proven methods for fluorescent labeling of POIs and only requires fusion of a small tag of 6-12 amino acids (aa) (~1 kDa). The tag contains four cysteines that bind to externally added, cell-permeable FlAsH and ReAsH biarsenical ligands, resulting in fluorescence.^{37,38} In several cases, this system results in less perturbation of POI localization^{39,40} or enzymatic activity⁴¹ compared to fusion with large fluorescent proteins. Additionally, protocols have been developed to allow for simultaneous detection of two POIs.⁴² These advantages have resulted in the extensive use of the tetracysteinebiarsenical system for live-cell imaging of intracellular proteins in a wide variety of cellular systems. 43 However, there are surprisingly few examples of its application to high-throughput library screening, 44,45 most likely due to the fact that the sensitivity of the tetracysteine-biarsenical system is at least an order of magnitude lower than that of green fluorescent protein.⁴⁵ Consequently, the system may have limited signalto-noise ratio when used for the detection of low expressing POIs, which is not uncommon when expressing heterologous proteins.

Examination of the aforementioned intracellular protein detection methods reveals a trade-off between sensitivity and impact on POI expression and/or its function. We recognized that this trade-off could be overcome by directly staining intracellular proteins with antibodies followed by flow cytometry analysis, however such an approach has not been developed for yeast. Compared to fusion of the POI with a large reporter protein, the use of antibodies for yeast intracellular POI detection minimizes the likelihood of perturbing POI function because antibody-POI binding can be accomplished by the use of small epitope tags (6-14 aa)commonly used in Western blot (i.e., c-Myc, flag, V5, HA, His, etc.). In the event that even small tags unacceptably affect the POI, as has been reported in some cases, 46 detection can be accomplished with POI-specific antibodies, abolishing the need for any POI modification. In addition, the diversity of fluorophore-antibody conjugates offers a wide range of brightness and spectral properties, allowing for the detection of low expressing POIs as well as multiple POIs simultaneously. Coupled with flow cytometry, such an antibody-based yeast intracellular staining (yICS) approach represents a sensitive, multiplexed, and high-throughput means for library screening.

In this study, we developed the yICS method that allows antibodies to directly access yeast intracellular compartments while maintaining cellular integrity for analysis by flow cytometry. In the first successful attempt of antibody-based flow cytometric detection of yeast intracellular proteins, we

demonstrate that yICS enables quantitative and reproducible detection of the yeast house-keeping proteins β actin and glyceraldehyde 3-phophate dehydrogenase (GAPDH). As a proof of concept, we then applied yICS to characterize and engineer a recombinant oxidoreductase pathway cloned from Scheffersomyces stipitis consisting of the xylose reductase (XR), xylitol dehydrogenase (XDH), and xylulokinase (XK) enzymes for direct conversion of xylose to ethanol in the yeast S. cerevisiae. yICS enabled simultaneous detection of all three pathway enzymes. Furthermore, the single-cell nature and sensitivity of vICS revealed clear variation in expression profiles depending on whether the enzyme expression cassettes were present on plasmids or integrated into the genome. Moreover, yICS enabled an 8.4-fold improvement in XDH activity, a known bottleneck in the pathway, by rapidly identifying rare (~1%) high-XDH producers in two consecutive rounds of CRISPR-mediated multicopy integration of XDH into the yeast δ site. These results demonstrate the utility of yICS to greatly accelerate the development of cellular pathways.

■ RESULTS AND DISCUSSION

Yeast Intracellular Staining (yICS) Design and Feasibility. The success of the yICS procedure hinges on enabling antibody access to intracellular compartments while maintaining cellular integrity for flow cytometry analysis. As the large size of antibodies prevents them from penetrating the cell wall of S. cerevisiae, 47 the first and most critical step of the yICS procedure is the complete removal of the cell wall by exposing the yeast cells to enzymes possessing mannase and β -1,3-glucanase activities (Figure 1A, Step 1). Immediately following cell wall removal, a fixation step is performed to stabilize the resulting fragile spheroplasts and to immobilize intracellular antigens for subsequent procedures (Figure 1A, Step 2). Next, antibody access to intracellular compartments is afforded by detergent permeabilization of cellular membranes (Figure 1A, Step 2). Antibody staining of intracellular proteins of interest (POIs) can then proceed (Figure 1A, Step 3), followed by detection of POIs using flow cytometry (Figure 1A, Step 4).

To test the feasibility of the yICS procedure, we first examined if fragile yeast spheroplasts could maintain their cellular integrity and be detected during flow cytometric analysis. To this end, yeast cells were grown to mid log phase, treated with lyticase enzyme (see Methods) to remove the cell wall, and observed under a microscope. In contrast to untreated cells (Figure 1B, left), lyticase-treated cells had a spherical shape and lacked protruding buds (Figure 1B, middle), both of which are characteristic of spheroplast formation. 48 In addition, the lyticase-treated sample showed some cellular debris (data not shown), presumably due to spheroplast lysis. This is not surprising as it is known that yeast cells lacking their cell wall are fragile and prone to lysis, especially when subjected to osmotic shock. 49,50 Indeed, lyticase-treated cells that were briefly exposed to hypotonic conditions (i.e., water) showed clumps of debris and were virtually absent of intact cells (Figure 1B, right), providing further evidence that lyticase treatment resulted in spheroplast

After confirming spheroplast formation, samples were fixed with 1% formalin under isotonic conditions (i.e., 1 M sorbitol) and subjected to flow cytometry analysis. Examination of the forward scatter (FSC) and side scatter (SSC) revealed that,

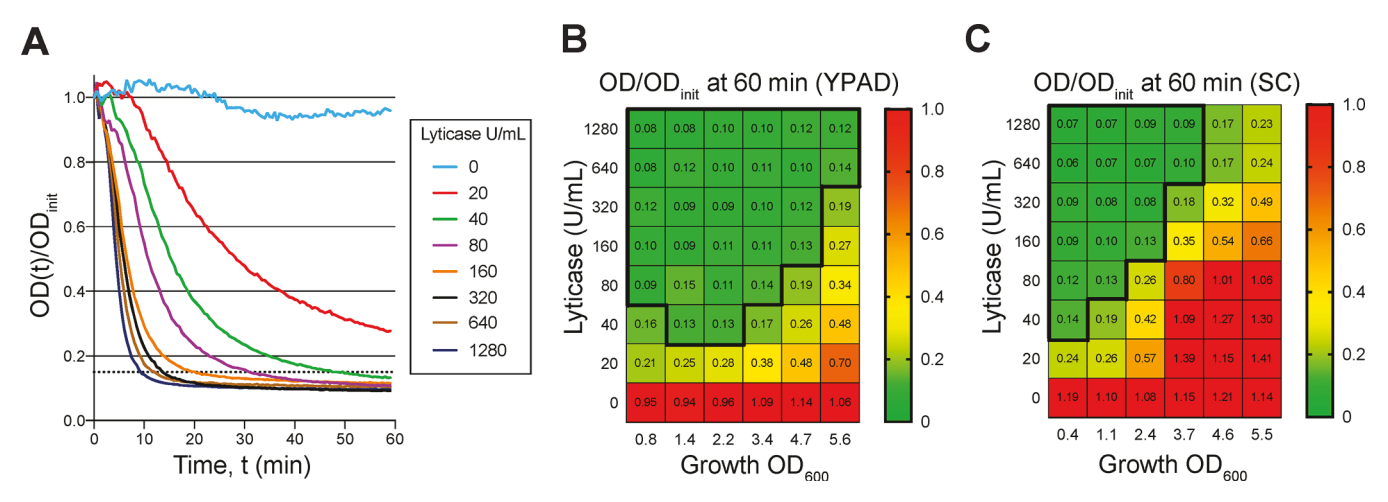


Figure 2. Development of high-throughput cell wall removal condition compatible with cells grown overnight in 96-well plate format. (A) 5 million cells from a culture grown overnight in YPAD to an OD_{600} of 2.2 were subjected to varying lyticase concentrations under hypotonic conditions, and spheroplast formation was monitored over time using the ratio of the OD_{600} at time t and the initial OD_{600} at t=0 of the reaction mixture $OD(t)/OD_{init}$. The dotted line represents $OD(t)/OD_{init} = 0.15$, the selected benchmark for adequate cell wall removal. (B,C) OD/OD_{init} values after 60 min treatment with a range of lyticase concentrations for cells grown to various OD_{600} in either YPAD media (B) or synthetic complete (SC) media (C). Color bar indicates OD/OD_{init} values. Cell wall removal conditions achieving $OD/OD_{init} \le 0.15$ are outlined in bold.

compared to untreated cells (Figure 1C, left, R1), lyticasetreated cells formed a distinct population (Figure 1C, middle, R2) characterized by lower FSC. This result was somewhat surprising because FSC intensity is generally thought to be indicative of cell size, yet the size of spheroplasts did not appear significantly altered when observed under a microscope (Figure 1B, left and middle). Instead, this reduced FSC intensity is likely due to altered optical properties of cells after cell wall removal, as supported by reports of spheroplasts appearing darker compared to nonspheroplasts when visualized by phase contrast microscopy.⁵¹ Importantly, about 50% of lyticase-treated cells (Figure 1C, middle, R2) were distinct from the lysed spheroplast population (Figure 1C, right, R3), confirming that a substantial fraction of spheroplasts remain intact during flow cytometry analysis. Taken together, these results indicate that formalin-fixed yeast spheroplasts can maintain their structural integrity and are readily detectable by flow cytometry, demonstrating the feasibility of the yICS procedure (Figure 1A).

Development of a High-Throughput yICS Workflow. After verifying that intact spheroplasts can be detected by flow cytometry, we next sought to develop a high-throughput yICS procedure that would permit the screening of large libraries. While antibody staining and flow cytometry can all be performed in 96-well format, cell wall removal typically involves a time-consuming preculture step (~4 h) in tubes or flasks to grow cells to mid-log phase, limiting the throughput of yICS-based screening and extending the duration of the yICS procedure beyond the length of a conventional workday. A convenient solution is to culture picked colonies overnight directly in 96-well plates and perform the yICS procedure the following morning. However, a significant challenge of this approach is that the resulting cell growth (hereafter referred to as growth OD₆₀₀) exceeds the mid-log phase (\sim 0.5-1.0 OD₆₀₀) that is optimal for cell wall removal. 49,50 Indeed, colonies picked directly into wells of a 96-well plate and grown overnight in rich YPAD media resulted in growth OD₆₀₀ ranging from 3.4 to 5.6 (Supplemental Figure S1), making complete cell wall removal more challenging. Therefore, it is essential to establish a robust cell wall removal protocol that can achieve satisfactory cell wall removal over a wide range of growth ${\rm OD}_{600}$.

To this end, we first set out to define a quantitative metric for satisfactory cell wall removal. Cells were grown to a growth OD_{600} of 2.2 in rich YPAD media in a 96-well plate and then cell wall removal was performed on 5 million cells using a range of lyticase concentrations under hypotonic conditions. Cell wall removal efficiency was assessed using the ratio between the OD₆₀₀ during lyticase treatment and the initial OD_{600} ($\mathrm{OD}/\mathrm{OD}_{\mathrm{init}}$), as previously reported.^{49,50} With no lyticase addition, the OD/OD_{init} ratio remained near 1 for the entirety of the 60 min (Figure 2A), suggesting that no cell lysis and hence no spheroplast formation had taken place. In contrast, the $\mathrm{OD}/\mathrm{OD}_{\mathrm{init}}$ ratio of lyticase-treated samples declined with increasing lyticase concentrations and longer treatment time. For lyticase concentrations ≥ 80 U/mL, the OD/OD_{init} ratio stabilized near 0.1, suggesting this value correlates with complete cell wall removal. Consequently, we designated that cell wall removal conditions achieving OD/ $OD_{init} \le 0.15$ (Figure 2A, dotted line) were satisfactory for future experiments. Furthermore, treatment with lyticase concentrations \geq 160 U/mL were able to achieve OD/OD_{init} \leq 0.15 in less than 20 min, suggesting these conditions can accommodate higher growth OD_{600} within a reasonable time frame.

We next evaluated the range of growth OD_{600} that could achieve satisfactory cell wall removal $(OD/OD_{init} \leq 0.15)$ with 60 min of lyticase treatment, which we deemed was a reasonable duration for step 1 of the yICS procedure (Figure 1A). Cells were grown in YPAD media from a serially diluted colony in a 96-well plate to yield growth OD_{600} values from 0.8 (mid-log phase) to 5.6 (the highest growth OD_{600} observed after overnight growth, Supplemental Figure S1). The OD/OD_{init} ratio after 60 min of lyticase treatment is recorded and color coded in Figure 2B. As growth OD_{600} increases, a higher lyticase concentration is required to achieve $OD/OD_{init} \leq 0.15$ (Figure 2B, bold boundary). However, for the two highest lyticase concentrations tested (640 and 1280 U/mL), $OD/OD_{init} \leq 0.15$ was achieved for all growth OD_{600} values tested (Figure 2B, top two rows). Thus, satisfactory cell wall removal

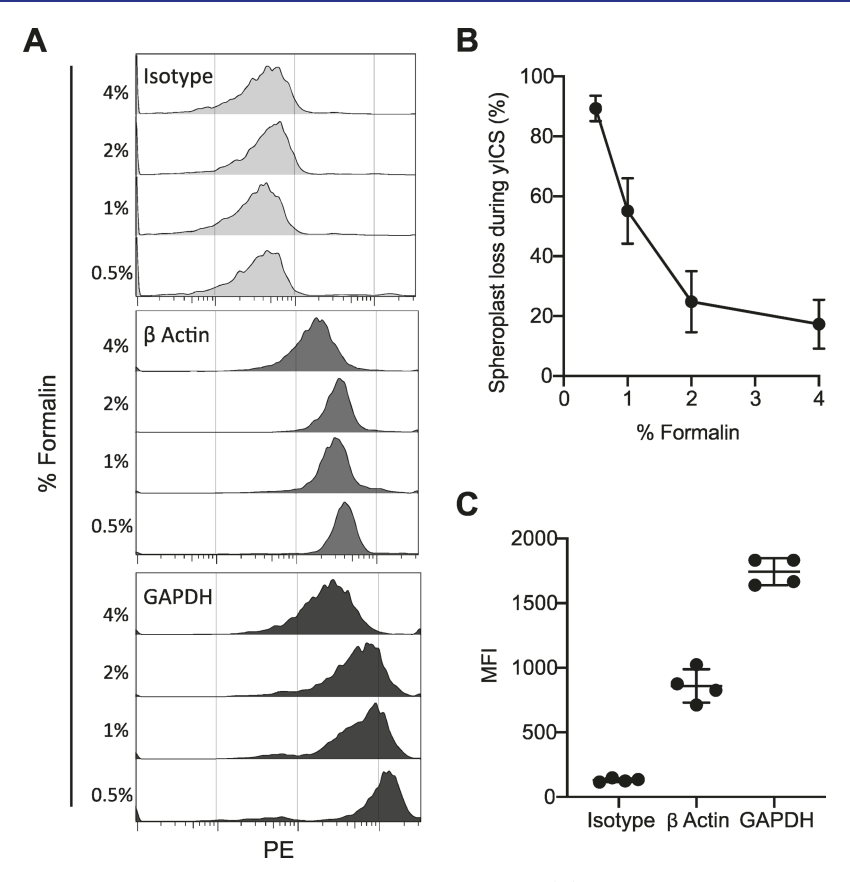


Figure 3. Detection of unmodified yeast intracellular housekeeping proteins by yICS. (A) Histograms of PE signal intensity of gated spheroplasts fixed with 0.5–4% formalin and stained for either a nonspecific isotype control (top panel), anti-β actin (middle panel), or anti-GAPDH (bottom panel) antibodies followed by a PE-conjugated secondary antibody. (B) The mean percentage of spheroplasts lost during the yICS procedure was calculated as the ratio of the number of gated intact spheroplasts detected by flow cytometry and the number of cells subjected to yICS as measured by OD₆₀₀. (C) The median fluorescence intensity (MFI) of four replicates from a single overnight culture fixed with 0.5% formalin and stained as in A. For B and C, error bars represent standard deviation of n = 3 and n = 4, respectively.

can be accomplished for cells grown overnight in 96-well format using a 60 min treatment with 1280 U/mL lyticase. This condition was used for subsequent experiments for cells grown in YPAD.

A parallel analysis was conducted for cells grown overnight in synthetic complete (SC) media, which is commonly used to maintain plasmid selection pressure. Compared to cells grown in YPAD (Figure 2B), cells grown in SC media were overall more resistant to cell wall removal, requiring either more lyticase or a lower growth OD_{600} to achieve $\mathrm{OD}/\mathrm{OD}_{\mathrm{init}} \leq 0.15$ (Figure 2C, bold boundary). Notably, no tested lyticase concentration was able to adequately remove the cell wall within 60 min for growth $\mathrm{OD}_{600} > 3.7$ (Figure 2C, right two columns). On the basis of this finding, a dilution step was incorporated in subsequent experiments when seeding colonies in SC media to ensure growth OD_{600} is < 3.7 to allow satisfactory cell wall removal in a 96-well format.

These results indicate that efficient cell wall removal can be achieved over a wide range of growth conditions, but is highly affected by media choice and cell growth stage in agreement with other reports. ^{49,50} In particular, it appears the yICS procedure is incompatible with stationary phase cells, due to the difficulty in removing their cell wall. Potentially explaining these findings, it has been demonstrated that the composition and mass of the cell wall are highly dynamic, changing with media, growth phase, temperature, and carbon source. ⁵² Therefore, we recommend that investigators perform similar

experiments to ensure satisfactory cell wall removal under their desired experimental conditions.

Validation of yICS Using Yeast Housekeeping Proteins. To validate the ability of yICS to detect intracellular POIs, we chose to detect the abundant yeast housekeeping proteins β actin and GAPDH, both of which have commercial antibodies readily available and thus allowing for their detection by yICS without any protein modification. Single yeast colonies were directly seeded into a 96-well plate in YPAD media and grown overnight. Following the yICS procedure shown in Figure 1A, the cell wall was removed using the optimal condition (i.e., 60 min treatment with 1280 U/mL lyticase) to generate spheroplasts which were then fixed with formalin and permeabilized with saponin. Permeabilized spheroplasts were stained with primary antibodies specific for β actin, GAPDH, or with a nonspecific isotype control followed by a phycoerythrin (PE)-conjugated secondary antibody and subjected to flow cytometry analysis. During the fixation step, a range of formalin concentrations (0.5-4% at room temperature for 30 min) was tested in anticipation of the opposing effects of fixation on antibody binding (i.e., fluorescence signal) and spheroplast structural integrity.

Notably, under all fixation conditions tested, a positive staining population was observed for both β actin and GAPDH compared to the background autofluorescence peak for the isotype control (Figure 3A). This result validates the ability of yICS to detect unmodified intracellular proteins and, to our

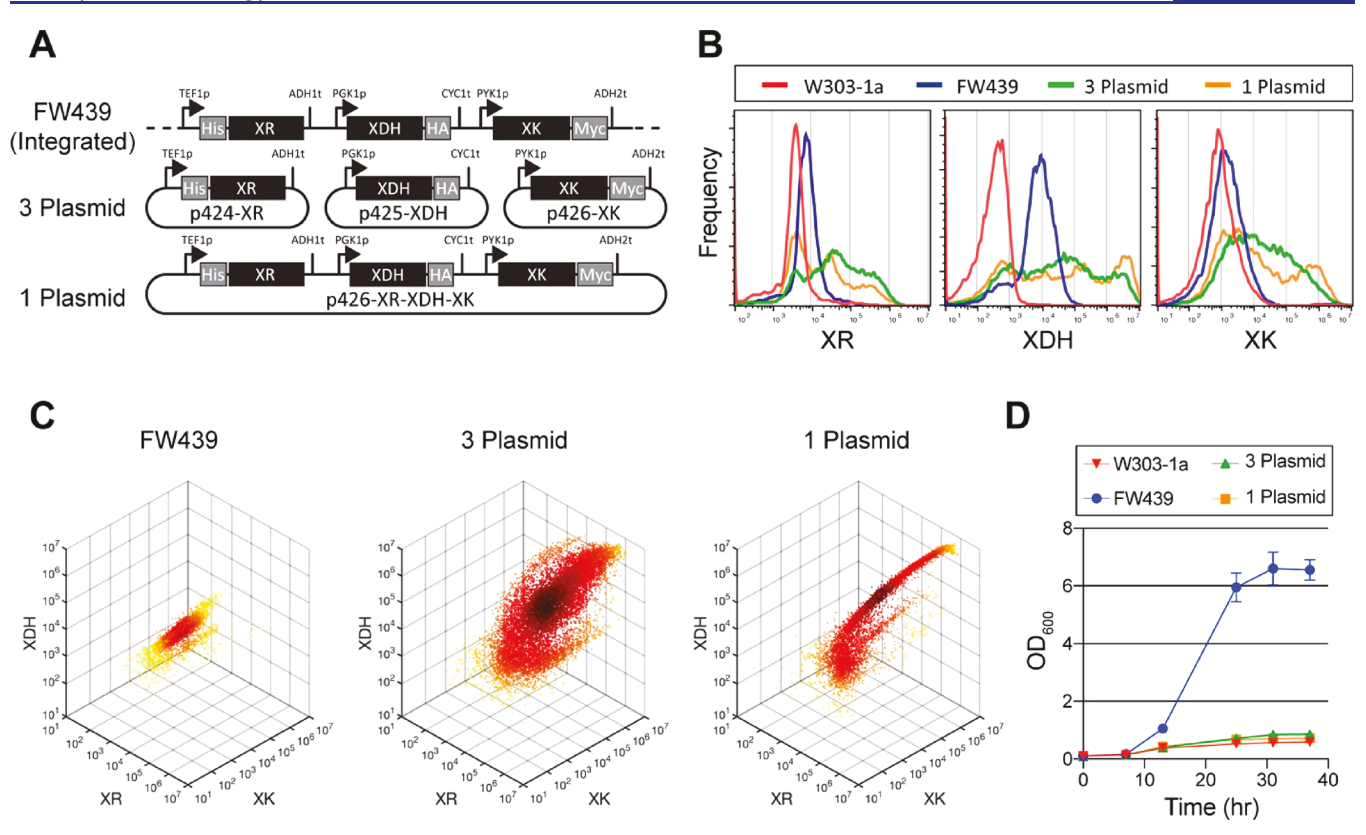


Figure 4. yICS characterization of recombinant xylose assimilation pathway. (A) XR, XDH, and XK pathway enzymes were tagged with His, HA, and c-Myc tags, respectively, and constitutively expressed from genes either integrated into the genome (top, strain FW439), on their own respective plasmid (middle, 3 plasmid), or on a single plasmid (bottom, 1 plasmid). Promoters and terminators for each gene are indicated by arrows and lines, respectively. (B) Histogram overlays of yICS signal for constructs in A simultaneously stained with anti-His, anti-HA, and anti-C-Myc antibodies to detect XR, XDH, and XK, respectively. Parental strain W303-1a was included as negative control. (C) Individual cells from B are plotted in three dimensions, with each axis representing the fluorescence signal intensity of XR, XDH, or XK. Coloring represents local cell density. (D) Aerobic growth curves with xylose as sole carbon source for constructs in A. Error bars represent mean \pm standard deviation, n = 2.

knowledge, is the first demonstration of antibody-based detection of yeast intracellular POIs using flow cytometry. Note that, although actin is the most abundant protein in eukaryotic cells, 53 the fact that β actin showed lower overall signal compared to GAPDH highlights that signal intensity is a function of several variables beyond protein abundance such as antibody affinity, antibody concentration, and antibody accessibility to its epitope. Therefore, comparing the abundance of different proteins using yICS requires an additional fluorescence quantification step. 20 As anticipated, fixation with higher formalin concentrations resulted in both slightly increased background autofluorescence signal (Figure 3A, top) and reduced fluorescence signal for both β actin and GAPDH (Figure 3A, middle and bottom), likely due to decreased antibody binding affinity for cross-linked epitopes as has been reported elsewhere.⁵⁴ As a result, the lowest formalin concentration (i.e., 0.5%) yielded the best signal-to-noise ratio. However, a more significant loss of spheroplasts was observed at lower formalin concentrations, with the 0.5% formalin fixation losing nearly 85% of spheroplasts while the 4% formalin fixation lost about 10% (Figure 3B). We attributed this loss to the weaker structural integrity of the spheroplasts fixed at the lower formalin concentrations, leading to their lysis during the washing steps in the subsequent antibody staining process. Despite the significant spheroplast loss using 0.5% formalin fixation, the large number of stained yeast cells (0.2 OD₆₀₀, equivalent to 5 million cells) and the high acquisition rate of flow cytometry (5000-10000 events per second) still

allow for rapid measurement of a sufficient number of intact spheroplasts for meaningful statistical analysis. Therefore, to ensure the best signal-to-noise ratio for quantitative measurement of yeast intracellular POIs, we chose to use the 0.5% formalin fixation condition and to acquire at least 30 000 events (~1 min per sample) for future experiments. Note that, while this fixation condition was optimal for our experimental system, the trade-off between signal-to-noise ratio and spheroplast loss should be evaluated on a case-by-case basis. Furthermore, while not investigated in this work, a fixation step can be performed before cell wall removal to minimize the effects of spheroplast formation on the metabolic and POI state in the cells.

Using the optimized 0.5% formalin fixation condition, the reproducibility of the yICS procedure was examined. A single colony was grown overnight in a 96-well plate and then split into four replicates. Following cell wall removal, formalin fixation, saponin permeabilization, and antibody staining (anti-GAPDH, anti- β actin, or an isotype control), the samples were subjected to flow cytometry analysis. The median fluorescence intensity (MFI) of the spheroplasts in each replicate showed a tight distribution with coefficients of variation (CVs) of 10.9%, 15.0%, and 6.0% for isotype control, β actin, and GAPDH, respectively (Figure 3C). Therefore, the yICS approach demonstrates the necessary reproducibility critical for characterizing and engineering recombinant pathways in yeast.

Characterization of a Recombinant Three-Enzyme Pathway Using yICS. As a proof of concept, we next applied

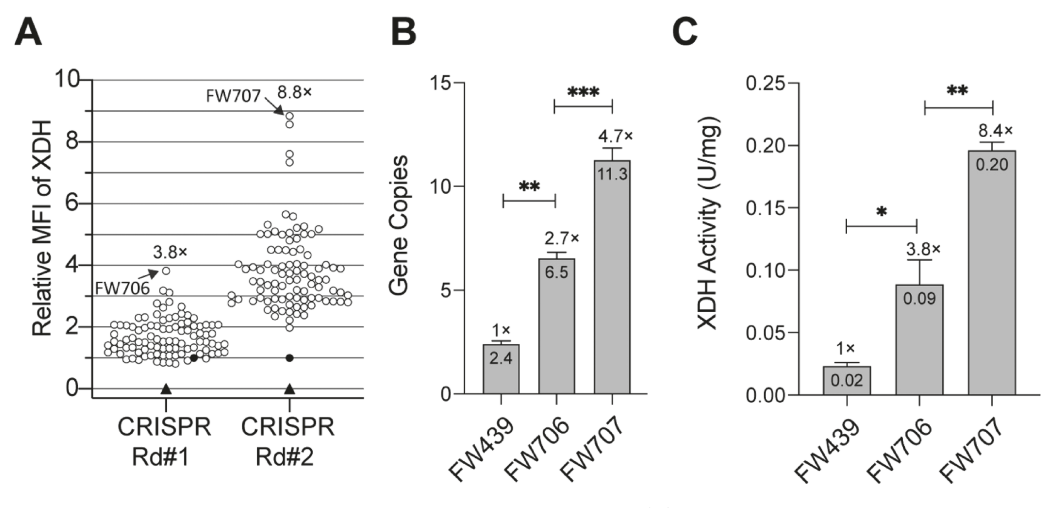


Figure 5. High-throughput yICS screening identifies high-expressing XDH clones. (A) XDH MFI of clones resulting from CRISPR-mediated integration of XDH expression cassette into FW439 (CRISPR Rd#1) and FW706 (CRISPR Rd#2) normalized to FW439. FW439 and W303–1a are indicated by filled black circles and triangles, respectively. (B) XDH gene copy numbers of selected strains quantified by qPCR. (C) Units of XDH activity per mg of protein in cleared cell lysate for selected strains. One unit of XDH activity is defined as the amount of XDH that reduces 1 μ mol of NAD⁺ to NADH per minute (see methods). Fold change of FW706 and FW707 compared to FW439 is indicated in each figure. For B and C, data represent mean \pm standard deviation, n=3; statistical comparisons computed by one-way ANOVA followed by *post hoc* Tukey's pairwise comparisons, *p<0.05, **p<0.01, ***p<0.01.

yICS to characterize the heterologous oxidoreductase D-xylose assimilation pathway important for converting xylose, a major component of renewable biomass (30-40%),5 ethanol. Specifically, we investigated the relationship between the expression levels of the three enzymes in the pathway (i.e., XR, XDH, and XK) and the ability of the cells to grow when using xylose as the sole carbon source. Variations in these three enzyme expression levels were achieved in yeast W303-1a by expressing them from genes either (1) integrated into the genome (Figure 4A, FW439), (2) on their own individual plasmids (Figure 4A, 3 plasmid), or (3) all on the same plasmid (Figure 4A, 1 plasmid). As is often the case when expressing proteins from nonmodel organisms, commercial antibodies specific for XR, XDH, and XK are unavailable. Thus, small epitope tags His (HHHHHHH), HA (YPYDVP-DYA), and c-Myc (EQKLISEEDL) were appended to XR, XDH, and XK, respectively, to enable multiplexed yICS detection while minimizing the probability of affecting enzyme function (Figure 4A).

Single colonies representing the three expression constructs as well as the W303-1a parental strain were diluted in appropriate glucose-containing SC dropout media and grown overnight in a 96-well plate. Spheroplasts were then prepared following the yICS procedure as described above, stained simultaneously for XR (anti-His PE), XDH (anti-HA Alexafluor 647), and XK (anti-c-Myc-biotin followed by streptavidin PE-Cy7), and analyzed by flow cytometry. As shown in Figure 4B, all three expression constructs showed positive signals for all three enzymes when compared to the W303-1a parental strain, validating the use of epitope tags for multiplexed yICS detection of yeast intracellular POIs. The signal distribution for both plasmid-bearing strains was much broader with ~25-50% of the cells expressing enzyme at higher levels than that of the FW439 integration strain, likely due to the heterogeneity in the ability of yeast cells to maintain high copy number (40–60) of these 2μ plasmids. Interestingly, the 3-plasmid and 1-plasmid strains showed very similar expression profiles for each enzyme despite evidence in the literature that the maintenance of plasmids is burdensome. 58,59

While FW439 showed only slightly increased XR and XK signal compared to W303–1a, *in vitro* activity assay with cell lysates detected significant activity for both enzymes, confirming their expression in FW439 (Supplemental Figure S2).

In addition to the insights gained by analyzing enzyme expression in isolation (Figure 4B), multiplexed yICS staining enables simultaneous evaluation of all enzyme levels in single cells, revealing further distinctions in the expression profile. When individual cells are visualized on a three-dimensional density plot with each axis representing the fluorescent signal intensity of XR, XDH, or XK (Figure 4C), all three constructs align along the same imaginary axis (Supplemental Video S1), signifying that, while the magnitude of enzyme expression varies, the relative ratio of the three enzymes in each cell is similar across these three constructs. Interestingly, the 3plasmid strain clearly shows a looser distribution along the imaginary axis than the 1-plasmid strain (Figure 4C, middle and right), likely due to greater variations in maintaining three types of 2μ plasmids simultaneously across individual cells. Although an expected result, such an observation highlights the fidelity of the yICS method and demonstrates the power of multiplexed analyses to reveal additional findings that would not be possible studying single proteins individually.

To investigate how these different enzyme expression profiles affect the ability of the cells to grow on xylose, the various strains were grown in appropriate SC dropout media containing 2% glucose overnight and then inoculated into rich media containing 2% xylose in liquid shaking culture. Subsequent monitoring of cell growth revealed that, surprisingly, only the FW439 strain was able to grow on xylose (Figure 4D) despite the fact that the plasmid-bearing strains have ~25–50% of cells expressing higher levels of enzymes (Figure 4B,C). These results suggest that high expression of at least one of the enzymes is cytotoxic when the cells are grown on xylose. Supporting this, it has been reported that overexpression of XK from *S. stipitis* or its homologue in *S. cerevisiae* inhibits cell growth on xylose but does not affect growth on glucose, ^{60,61} potentially due to the generation of

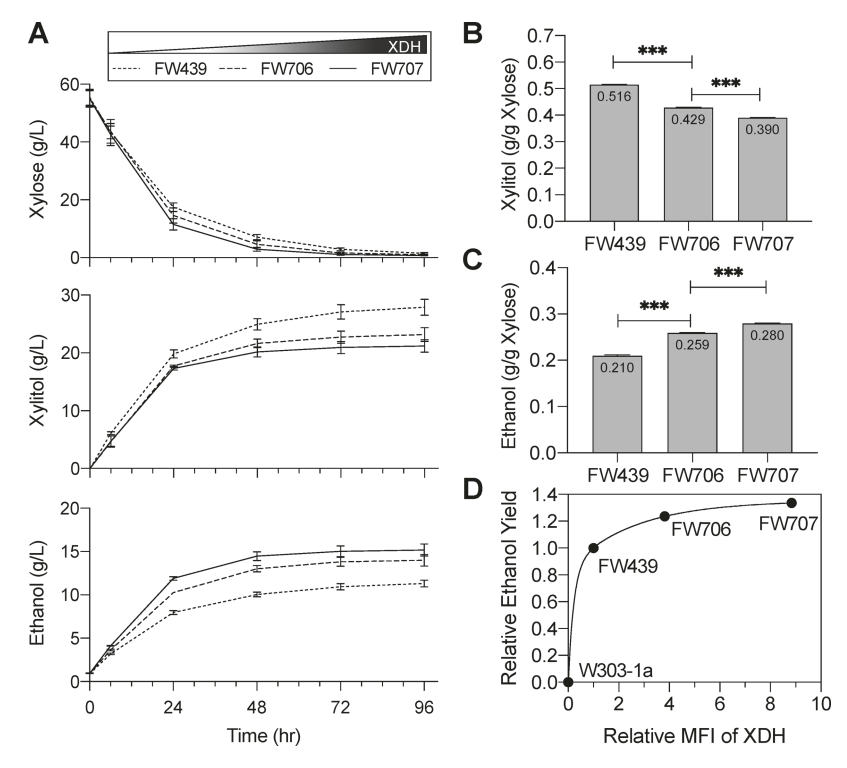


Figure 6. High-expressing XDH clones identified by yICS screening demonstrate enhanced performance during anaerobic xylose fermentation. (A) Concentrations of xylose (top panel), xylitol (middle panel), and ethanol (bottom panel) at indicated time points during fermentation. (B) Xylitol and (C) ethanol generated at 96 h of fermentation per xylose consumed (w/w). (D) Relative ethanol yield *versus* the relative XDH MFI normalized to FW439 for each strain fit with a two-phase association model. Data in A, B, and C represent mean \pm standard deviation, n = 2; statistical comparisons computed by one-way ANOVA followed by *post hoc* Tukey's pairwise comparisons, ***p < 0.001.

toxic byproducts and/or the depletion of ATP by XK activity. Regardless of the mechanism, the data suggest that enzyme expression levels need to be tightly controlled to maximize xylose utilization, which is a challenging task using plasmid-based expression due to their highly heterogeneous expression profile. Therefore, we chose FW439 for further engineering of the pathway to improve the xylose-to-ethanol conversion.

Engineering a Xylose Assimilation Pathway Using yICS. One of the frequently reported bottlenecks of the oxidoreductase D-xylose assimilation pathway is the low activity of XDH relative to XR, resulting in xylitol accumulation and limiting ethanol yield. 63,64 In an attempt to increase the XDH expression level and relieve this metabolic bottleneck, we performed CRISPR-mediated genome integration of XDH into the FW439 strain (see Methods). While high copy integrants are commonly identified by G418 resistance afforded by cointegration of the KanMX gene,65 strain FW439 already contained several copies of KanMX by utilizing this technique, necessitating an alternative screening approach. To this end, single colonies resulting from the transformation were grown overnight in YPAD media in a 96-well plate (94 transformants plus W303-1a and FW439) and subjected to yICS analysis to identify high XDH producers. As shown in Figure 5A, CRISPR Round 1, 68, of the 94 XDH transformants (i.e., ~72%) showed statistically increased MFI compared to the parental FW439 strain (p < 0.05, assuming a CV of 15%). The highest XDH-expressing clone, FW706, showed nearly a 4-fold increase in MFI and was chosen for a second round of CRISPR-mediated genome integration of XDH. yICS screening was performed on the resulting library, including W303-1a and FW439 as controls to account for batch variation.

Following normalization to FW439, about half of the transformants had a considerably lower relative MFI than the FW706 parent strain (Figure 5A, CRISPR Round 2), potentially due to the unstable nature of tandem multicopy integrations. Nevertheless, the best clone, FW707, showed nearly a 9-fold increase in MFI over the FW439 strain. The rarity of these "jackpot" clones expressing very high levels of XDH (~1% in each round) would make their identification very laborious, if not impossible, using common but lower-throughput approaches such as Western blot 66,67 or *in vitro* activity assays. 88,69 Therefore, the use of yICS can greatly accelerate the clonal selection process based on the expression level of POIs.

Subsequent qPCR analysis of the selected strains revealed that the increase in MFI following each round of CRISPR integration was accompanied by a significant increase in the XDH copy number (p < 0.01), with about 4 additional XDH copies being introduced in the highest expressing clone per round (Figure 5B). Note that within the CRISPR Round 2 library, the best clone, FW707, was confirmed to have two more copies than the second-best clone (p < 0.05) highlighting the superb resolution of yICS for identifying subtle changes in POI expression level. The best clones from each CRISPR round were then evaluated for their XDH activity in vitro (see Methods), revealing a 2-4 fold increase in activity with each round of XDH integration (p < 0.05) (Figure 5C). Taken together, these results demonstrate the ability of yICS to rapidly and accurately identify clones of interest based on protein expression level, reducing the library size to more manageable levels that allow further pathway evaluation using more direct, but typically lower throughput, functional assays such as fermentation.

ACS Synthetic Biology Research Article pubs.acs.org/synthbio

Accordingly, the selected strains FW706 and FW707 were next subjected to low-throughput anaerobic xylose fermentation to compare their performance to the FW439 parental strain. While strains with higher XDH expression had a slightly increased rate of xylose consumption (Figure 6A, top), xylitol accumulation was significantly reduced (Figure 6A, middle), signifying increased in vivo activity of XDH. Specifically, xylitol accumulation was reduced by 24% in FW707 compared to FW439 upon xylose depletion (96 h) (0.516 versus 0.390 g/g xylose consumed, Figure 6B). More importantly, increased XDH expression led to improved ethanol production (Figure 6A, bottom) with FW707 achieving a 33% increase in ethanol yield compared to FW439 (0.280 versus 0.210 g/g xylose consumed, Figure 6C). While these data clearly demonstrate that the XDH activity is indeed a bottleneck in the pathway, they raise the question of whether further increases in XDH activity can continue to drive efficient increases in ethanol yield. To this end, the relative MFI of XDH was plotted against the relative ethanol yield for each strain (Figure 6D). While the number of data points is small, these data indicate that further XDH integrations will likely lead to diminishing returns and suggest the use of alternative strategies beyond tuning XDH expression to achieve further improvement of xylose-to-ethanol conversion. Taken together, these results demonstrate that the knowledge of protein expression level, as provided by yICS, can give significant insights into clone performance and highlight the use of yICS in the pathway engineering pipeline as a versatile tool that can fulfill both rapid screening as well as detailed strain characterization.

In conclusion, there is an unmet need for methods that can facilitate rapid library screening when desirable cellular phenotypes cannot be directly linked to fluorescence or growth advantages. While screening approaches based on protein expression level or activity can be a reliable indicator of cellular performance, current methods for measuring these parameters in yeast, such as Western blot or in vitro activity assay, do not have the throughput to handle large libraries. To this end, we developed and demonstrated for the first time a flow cytometric approach that enables the rapid detection and quantification of yeast intracellular POIs via antibody staining with little (Figure 4B,C) to no (Figure 3A) POI modification. The compatibility of this yICS approach with multiwell plate format enabled the rapid identification of rare (~1%), high-XDH producers from a library of XDH integrants (Figure 5A), a feat that would have been especially tedious using Western blot or in vitro activity assay. Furthermore, the single-cell resolution of flow cytometry coupled with the diversity of available fluorophores enables multiplexed characterization of several POIs simultaneously (Figure 4B,C), revealing valuable information on population heterogeneity and the relative ratio of multiple enzymes in individual cells. In addition to the applications presented here, the dual capability of yICS to perform detailed characterization as well as rapid screening opens up numerous opportunities. For example, pathway flux can now be maximized by tuning the ratios of multiple enzymes simultaneously, greatly expediting the clonal selection process. For these reasons, we believe that the yICS method developed here is useful whenever a sensitive, high-throughput, and quantitative measurement of intracellular proteins is required.

METHODS

Strains, Plasmids, Reagents, and Cell Culture Conditions. The strains and plasmids used in this study are summarized in Table S1. All yeast strains were constructed from S. cerevisiae W303-1a (ATCC 208352) as described in SI Methods. PCR primers were synthesized by Integrated DNA Technologies (Coralville, IA) and are listed in Table S2. All chemicals and reagents were purchased from Sigma-Aldrich (St. Louis, MO) unless specified otherwise. Nonplasmidbearing yeast strains were grown in either YPAD medium (10 g/L yeast extract, 20 g/L peptone, 100 mg/L adenine sulfate, 20 g/L glucose), YPAX medium (10 g/L yeast extract, 20 g/L peptone, 100 mg/L adenine sulfate, 20 g/L xylose), or yeast synthetic complete (SC) medium (1.67 g/L of yeast nitrogen base (Difco, Detroit, MI), 5 g/L ammonium sulfate, 20 g/L glucose, 100 mg/L adenine sulfate, and 0.64 g/L of CSM (MP Biomedicals, Solon, OH)). Plasmid-bearing yeast strains were grown in appropriate SC dropout medium (same recipe as SC medium except that CSM dropout powder was used in place of the CSM powder). Yeast cells were grown at 30 °C in an orbital shaker at 225 rpm unless specified otherwise. Cell concentrations were determined as OD_{600} measurements using a SpectraMax M5 plate reader (Molecular Devices, Sunnyvale, CA) and standard curve (1 OD₆₀₀ is calibrated to equal 25 million cells). All centrifugation steps were performed at 3200g for 3 min.

General yICS Procedure. To perform cell wall removal in 96-well plate format, yeast strains were seeded directly from a single colony into individual wells of the plate and grown for 16 h at 30 °C without shaking. For strains grown in SC or SC dropout medium, colonies were diluted 10-fold before seeding to ensure growth OD_{600} < 3.7. Aliquots of 5 million cells (0.2) OD₆₀₀) were then transferred to wells of another 96-well plate, pelleted, and resuspended in 200 µL of 30 mM TCEP (Bond-Breaker Thermo Fisher Scientific, Waltham, MA) to reduce disulfide bridges and loosen the cell wall. After incubation at 30 °C without shaking for 20 min, cells were washed once in Milli-Q water (18.2 m Ω cm at room temperature), resuspended in 200 µL TMS buffer (50 mM Tris-HCl pH 7.4, 5 mM MgCl₂, 1 M sorbitol) with 3 mM TCEP and 1280 U/mL of lyticase from Arthrobacter luteus and incubated at 30 °C without shaking to initiate cell wall removal. To observe the progress of cell wall removal, cells were taken at desired time points and imaged using a Leica TCS SP8 MP inverted confocal microscope (Leica Microsystems, Wetzlar, Germany) in differential interference contrast (DIC) mode. After 60 min of lyticase treatment, the resulting spheroplasts were washed twice with 1 M sorbitol and fixed in 200 µL 1 M sorbitol with 0.5% formalin for 30 min at room temperature.

The formalin-fixed spheroplasts were then permeabilized in 200 µL saponin-based permeabilization buffer (eBioscience, San Diego, CA) for 30 min at room temperature, pelleted, and stained with primary antibodies at desired concentrations in 50 μ L permeabilization buffer for 1 h at room temperature. If a secondary antibody staining was required, spheroplasts were then washed twice in 200 µL permeabilization buffer, resuspended in 50 µL of permeabilization buffer containing the secondary antibody at the desired concentration, and incubated for 1 h at room temperature. After washing twice in 200 μ L permeabilization buffer, spheroplasts were resuspended to 0.5 million spheroplasts/mL in flow buffer (PBS pH 7.4, 0.5% bovine serum albumin) for flow cytometry analysis on

ı

either a MoFlow Astrios cell sorter (Beckman Coulter, Indianapolis, IN) or an Attune flow cytometer (Applied Biosystems, Foster City, CA). Flow cytometry data were analyzed using FlowJo (FlowJo LLC, Ashland, OR).

The 1280 U/mL lyticase concentration used for cell wall removal and the 0.5% formalin concentration used for spheroplast fixation were optimized for the specific system reported in this study as detailed in Figure 2 and Figure 3. Note that both concentrations should be optimized under new experimental conditions such as when investigating a different yeast strain or cell culture condition as detailed below.

Optimization of Lyticase Concentration. Five million $(0.2 \text{ }OD_{600})$ yeast cells grown from each new culture conditions are transferred to wells of a 96-well plate, and the cell wall removal protocol is performed as described above except for the following changes: (1) the lyticase digestion step is performed in 200 μ L TM buffer without sorbitol (50 mM Tris-HCl pH 7.4, 5 mM MgCl₂) to promote spheroplast lysis, (2) varying concentrations of lyticase is added to the TM buffer, and (3) during lyticase digestion, the OD₆₀₀ of the cells is measured and recorded every 30 s using a SpectraMax M5 plate reader at 30 °C with shaking to prevent cell settling. The OD/OD_{init} values are then evaluated to determine the optimal lyticase concentration as illustrated in Figure 2.

Optimization of Formalin Concentration via Detection of Yeast Housekeeping Proteins. After cell wall removal, spheroplasts are fixed with varying concentrations of formalin. Formalin concentrations of 0.5%, 1%, 2%, or 4% are commonly used in literature for different types of cells. 70,71 Note that other fixation reagents could also be considered. 72,73 Formalin-fixed spheroplasts are then permeabilized and stained for housekeeping proteins such as GAPDH and β actin as described above. The fluorescence intensity of housekeeping proteins and the autofluorescence intensity of the isotype control are next evaluated to determine the optimal formalin concentration as illustrated in Figure 3A. In this study, 20 μ g/ mL of either mouse anti-GAPDH antibody (clone MA5-15738, Invitrogen, Waltham, MA), mouse anti- β actin antibody (clone MA1-744, Invitrogen), or mouse IgG1κ isotype control (clone P3.6.2.8.1, eBioscience) were used as the primary antibodies; 2 µg/mL of PE-conjugated goat antimouse antibody (clone Poly4053, BioLegend, San Diego, CA) was used as the secondary antibody.

Detection and Characterization of XR, XDH, and XK. To detect XR, XDH, and XK enzymes all at once, the general yICS procedure was performed for W303–1a, FW439, 3-plasmid, and 1-plasmid strains as described above using a primary antibody cocktail containing 20 μ g/mL each of PEconjugated anti-His (clone J095G46, BioLegend), biotinconjugated anti-c-Myc (clone 9E10, BioLegend), and Alexafluor647-conjugated anti-HA (clone 16B12, BioLegend). Secondary antibody staining was performed with 2 μ g/mL PE-Cyanine7-conjugated streptavidin (eBioscience). MATLAB (MathWorks, Natick, MD) was used for three-dimensional visualization of flow cytometry data.

ylCS Screening of CRISPR Integration Library. FW439 was first transformed with p414-TEF1p-Cas9-CYC1t (Table S1) encoding a Cas9 expression cassette (a gift from George M. Church, Addgene plasmid #43802) and plated on SC-TRP. A single colony was picked from the plate and transformed simultaneously with p426gRNA-Delta (Table S1) encoding the guide RNA targeting the yeast δ site and linearized donor DNA containing the XDH expression cassette flanked by δ

sites produced from PCR amplification of p426-d-XDH-d (Table S2). Transformants were plated on SC-TRP-URA. FW439 and 95 transformants were subjected to the yICS procedure using 20 μ g/mL of Alexafluor647-conjugated anti-HA. The clone with the highest XDH expression was designated FW706. A second round of XDH integration into FW706 was performed as described above but with gRNA plasmid p423gRNA-Delta (Table S2). Transformants were plated on SC-TRP-HIS and screened using yICS to yield the best clone FW707.

Characterization of High XDH-Expressing Clones Selected by yICS Screening. The copy number of the XDH gene in strains FW439, FW706, and FW707 was determined using quantitative PCR (qPCR) by comparing the C_T values of the XDH gene to the reference gene phosphoglucose isomerase (PGI1) using previously described methods.⁷⁴ qPCR was performed on 7900HT (Applied Biosystems, Warrington, UK) with SYBR Green qPCR Master Mix (Applied Biosystems, Warrington, UK) containing 200 nM of qPCR primers (Table S2) and 200 ng genomic DNA isolated from each strain using the Wizard Genomic DNA kit (Promega, Madison, WI).

The in vitro XR, XDH, and XK activities were evaluated using the cell lysates of strains FW439, FW706, and FW707 prepared by Y-PER treatment (Yeast Protein Extraction Reagent, Pierce, Rockford, IL) following the manufacturer's protocol. Protein concentrations in cell lysates were determined using the BCA Protein Assay Kit (Thermo Fisher Scientific) following the manufacturer's protocol. Enzyme activities were determined by adapting previously described methods.^{75–77} Briefly, enzyme reactions were carried out at room temperature in 96-well plates in a total volume of 200 μ L. XR activity was evaluated in 50 mM potassium phosphate buffer (pH 7), 350 mM D-xylose, 0.02 mM NAD(P)H, and 50 μg cell extract; XDH activity was evaluated in a reaction mixture containing 50 mM Tris buffer (pH 9), 300 mM xylitol, 2 mM NAD⁺, and 25 μ g cell extract; and XK activity was evaluated in 50 mM Tris buffer at pH 7.5 containing 2 mM magnesium chloride, 8 mM sodium fluoride, 2 mM ATP, 1 mM phosphoenolpyruvate, 3 mM red glutathione, 0.3 mM NADH, 10 units of pyruvate kinase, 10 units of lactate dehydrogenase, 5 mM D-xylulose, and 10 µg cell extract. Reduction of NAD+ to NADH was monitored continuously by absorbance measurements at 340 nm for 5 min using a SpectraMax M5 plate reader. The absorbance change per minute $(\Delta A \text{ min}^{-1})$ was divided by the molar absorptivity of NAD(P)H (6.22 cm⁻¹ mmol⁻¹) to calculate substrate consumption per minute. One unit of enzyme activity is defined as the amount of enzyme that reduces 1 μ mol of NAD⁺ per minute in the reaction conditions described above.

The xylose-to-ethanol conversion capability of FW439, FW706, and FW707 was evaluated using anaerobic fermentation at 30 $^{\circ}$ C and 225 rpm. Ten OD₆₀₀ of yeast cells were inoculated into anaerobic YPA medium containing 55 g/L xylose with 0.01 g/L ergosterol and 0.4 g/L Tween-80 in an anaerobic chamber and sealed in serum bottles with butyl rubber stoppers. The glucose, xylose, xylitol, glycerol, acetate, and ethanol concentrations of fermentation samples were analyzed at indicated time points by high performance liquid chromatography (HPLC, Agilent Technologies 1200 Series, Santa Clara, CA) equipped with a refractive index detector and a Rezex ROA Organic Acid H $^+$ (8%) column (Phenomenex

Inc., Torrance, CA). The column was eluted with 0.005 N $\rm H_2SO_4$ flowing at 0.6 mL/min at 60 $^{\circ}$ C.

Statistical Analysis. Data are expressed as mean \pm standard deviation. Means were compared by one-way ANOVA followed by *post hoc* Tukey's pairwise comparisons using the software package Prism (GraphPad Software, San Diego, CA). Significance is indicated by *p < 0.05, **p < 0.01, ***p < 0.001.

ASSOCIATED CONTENT

Supporting Information

The Supporting Information is available free of charge at https://pubs.acs.org/doi/10.1021/acssynbio.0c00199.

Figure S1: Histogram of cell growth after overnight culture in 96-well plate; Figure S2: XR and XK enzyme activity in W303–1a and FW439; Table S1: Strains and plasmids used in this study; Table S2: Primers used in this study; Supplemental Methods: Cloning procedures, plasmid construction, and strain construction (PDF) Video S1: Overlay of 1 plasmid, 3 plasmid, and FW439 expression profiles of XR, XDH, and XK (MP4)

AUTHOR INFORMATION

Corresponding Author

Fei Wen – Department of Chemical Engineering, University of Michigan, Ann Arbor, Michigan 48109, United States;
ocid.org/0000-0001-7970-4796; Email: feiwenum@umich.edu

Authors

Brett D. Hill – Department of Chemical Engineering, University of Michigan, Ann Arbor, Michigan 48109, United States

Ponnandy Prabhu — Department of Chemical Engineering, University of Michigan, Ann Arbor, Michigan 48109, United States

Syed M. Rizvi — Department of Chemical Engineering, University of Michigan, Ann Arbor, Michigan 48109, United States

Complete contact information is available at: https://pubs.acs.org/10.1021/acssynbio.0c00199

Author Contributions

FW conceived and supervised the project. BDH, PP, SMR, and FW designed the experiments. BDH, PP, and SMR performed the experiments. BDH, FW, and PP analyzed the data and wrote the manuscript. All authors read and revised the manuscript.

Notes

The authors declare no competing financial interest.

ACKNOWLEDGMENTS

This work was supported by the National Science Foundation (NSF) CAREER Award 1653611 and the National Institutes of Health (NIH) grant OD020053. FW was additionally supported by the Rogel Cancer Center Support Grant (NIH P30 CA046592) and FW and BDH by the A. Alfred Taubman Medical Research Institute's Taubman Institute Innovation Projects program. We would like to acknowledge the University of Michigan DNA Sequencing Core for Sanger sequencing and qPCR analysis, the University of Michigan Flow Cytometry Core and CyTOF Core for use of flow cytometers, and the University of Michigan Microscopy Core

for providing access to the Leica SP8 confocal microscope. We would also like to acknowledge Zengyi Shao and George M. Church for providing the pRS-TEFp-KanMX-TEFt and p426-SNR52p-gRNA.CAN1.Y-SUP4t plasmids, respectively.

REFERENCES

- (1) Wang, H. H., Isaacs, F. J., Carr, P. A., Sun, Z. Z., Xu, G., Forest, C. R., and Church, G. M. (2009) Programming cells by multiplex genome engineering and accelerated evolution. *Nature* 460, 894–898.
- (2) Yuan, Y., Du, J., and Zhao, H. (2013) Customized optimization of metabolic pathways by combinatorial transcriptional engineering. *Methods Mol. Biol.* 985, 177–209.
- (3) Lu, C., and Jeffries, T. (2007) Shuffling of promoters for multiple genes to optimize xylose fermentation in an engineered Saccharomyces cerevisiae strain. *Appl. Environ. Microbiol.* 73, 6072–6077.
- (4) Si, T., Chao, R., Min, Y., Wu, Y., Ren, W., and Zhao, H. (2017) Automated multiplex genome-scale engineering in yeast. *Nat. Commun.* 8, 15187.
- (5) Begley, T. P., Wen, F., McLachlan, M., and Zhao, H. (2008) Directed Evolution: Novel and Improved Enzymes. In *Wiley Encyclopedia of Chemical Biology*, pp 1–10, John Wiley & Sons, Inc., Hoboken, NJ.
- (6) Zhou, S., and Alper, H. S. (2019) Strategies for directed and adapted evolution as part of microbial strain engineering. *J. Chem. Technol. Biotechnol.* 94, 366–376.
- (7) Lee, M. E., Aswani, A., Han, A. S., Tomlin, C. J., and Dueber, J. E. (2013) Expression-level optimization of a multi-enzyme pathway in the absence of a high-throughput assay. *Nucleic Acids Res.* 41, 10668—10678.
- (8) Young, E. M., Zhao, Z., Gielesen, B. E. M., Wu, L., Benjamin Gordon, D., Roubos, J. A., and Voigt, C. A. (2018) Iterative algorithm-guided design of massive strain libraries, applied to itaconic acid production in yeast. *Metab. Eng.* 48, 33–43.
- (9) Farasat, I., Kushwaha, M., Collens, J., Easterbrook, M., Guido, M., and Salis, H. M. (2014) Efficient search, mapping, and optimization of multi-protein genetic systems in diverse bacteria. *Mol. Syst. Biol.* 10, 731–731.
- (10) Zhu, J., Schwartz, C., and Wheeldon, I. (2019) Controlled intracellular trafficking alleviates an expression bottleneck in S. cerevisiae ester biosynthesis. *Metab. Eng. Commun. 8*, No. e00085.
- (11) Peng, B., Williams, T. C., Henry, M., Nielsen, L. K., and Vickers, C. E. (2015) Controlling heterologous gene expression in yeast cell factories on different carbon substrates and across the diauxic shift: a comparison of yeast promoter activities. *Microb. Cell Fact.* 14, 91.
- (12) Kim, H., Yoo, S. J., and Kang, H. A. (2014) Yeast synthetic biology for the production of recombinant therapeutic proteins. *FEMS Yeast Res.* 15, 1–16.
- (13) Hong, K.-K., and Nielsen, J. (2012) Metabolic engineering of Saccharomyces cerevisiae: a key cell factory platform for future biorefineries. *Cell. Mol. Life Sci.* 69, 2671–2690.
- (14) Bugada, L. F., Smith, M. R., and Wen, F. (2018) Engineering Spatially Organized Multienzyme Assemblies for Complex Chemical Transformation. *ACS Catal.* 8, 7898–7906.
- (15) Sun, J., Shao, Z., Zhao, H., Nair, N., Wen, F., Xu, J.-H., and Zhao, H. (2012) Cloning and characterization of a panel of constitutive promoters for applications in pathway engineering in Saccharomyces cerevisiae. *Biotechnol. Bioeng.* 109, 2082–92.
- (16) Li, Y., Li, S., Thodey, K., Trenchard, I., Cravens, A., and Smolke, C. D. (2018) Complete biosynthesis of noscapine and halogenated alkaloids in yeast. *Proc. Natl. Acad. Sci. U. S. A. 115*, E3922–E3931.
- (17) Nielsen, J., and Jewett, M. C. (2008) Impact of systems biology on metabolic engineering of *Saccharomyces cerevisiae*. *FEMS Yeast Res.* 8, 122–131.

- (18) Tan, S. Z., Manchester, S., and Prather, K. L. J. (2016) Controlling central carbon metabolism for improved pathway yields in Saccharomyces cerevisiae. *ACS Synth. Biol.* 5, 116–124.
- (19) Smith, M. R., Khera, E., and Wen, F. (2015) Engineering novel and improved biocatalysts by cell surface display. *Ind. Eng. Chem. Res.* 54, 4021–4032.
- (20) Smith, M. R., Gao, H., Prabhu, P., Bugada, L. F., Roth, C., Mutukuri, D., Yee, C. M., Lee, L., Ziff, R. M., Lee, J. K., and Wen, F. (2019) Elucidating structure—performance relationships in whole-cell cooperative enzyme catalysis. *Nat. Catal.* 2, 809–819.
- (21) Boder, E. T., and Wittrup, K. D. (2000) Yeast surface display for directed evolution of protein expression, affinity, and stability. *Methods Enzymol.* 328, 430–44.
- (22) Wen, F., Nair, N. U., and Zhao, H. (2009) Protein engineering in designing tailored enzymes and microorganisms for biofuels production. *Curr. Opin. Biotechnol.* 20, 412–419.
- (23) Crivat, G., and Taraska, J. W. (2012) Imaging proteins inside cells with fluorescent tags. *Trends Biotechnol.* 30, 8–16.
- (24) Chudakov, D. M., Matz, M. V., Lukyanov, S., and Lukyanov, K. A. (2010) Fluorescent proteins and their applications in imaging living cells and tissues. *Physiol. Rev.* 90, 1103–1163.
- (25) Los, G. V., and Wood, K. (2006) The HaloTag: a novel technology for cell imaging and protein analysis. *Methods Mol. Biol.* 356, 195–208.
- (26) Blackstock, D., and Chen, W. (2014) Halo-tag mediated self-labeling of fluorescent proteins to molecular beacons for nucleic acid detection. *Chem. Commun.* 50, 13735–13738.
- (27) Gautier, A., Juillerat, A., Heinis, C., Corrêa, I. R., Kindermann, M., Beaufils, F., and Johnsson, K. (2008) An engineered protein tag for multiprotein labeling in living cells. *Chem. Biol.* 15, 128–136.
- (28) Juillerat, A., Gronemeyer, T., Keppler, A., Gendreizig, S., Pick, H., Vogel, H., and Johnsson, K. (2003) Directed evolution of O6-alkylguanine-DNA alkyltransferase for efficient labeling of fusion proteins with small molecules in vivo. *Chem. Biol.* 10, 313–7.
- (29) Jensen, E. C. (2012) Use of Fluorescent Probes: Their Effect on Cell Biology and Limitations. *Anat. Rec.* 295, 2031–2036.
- (30) Heo, M., Nord, A. L., Chamousset, D., Van Rijn, E., Beaumont, H. J. E., and Pedaci, F. (2017) Impact of fluorescent protein fusions on the bacterial flagellar motor. *Sci. Rep.* 7, 12583.
- (31) Snapp, E. (2005) Design and Use of Fluorescent Fusion Proteins in Cell Biology. Curr. Protoc. Cell Biol. 27, 21.4.1–21.4.13.
- (32) Baens, M., Noels, H., Broeckx, V., Hagens, S., Fevery, S., Billiau, A. D., Vankelecom, H., and Marynen, P. (2006) The dark side of EGFP: Defective polyubiquitination. *PLoS One 1*, No. e54.
- (33) Margolin, W. (2012) The price of tags in protein localization studies. *J. Bacteriol.* 194, 6369–6371.
- (34) Swulius, M. T., and Jensen, G. J. (2012) The helical mreb cytoskeleton in Escherichia coli MC1000/pLE7 is an artifact of the N-terminal yellow fluorescent protein tag. *J. Bacteriol.* 194, 6382–6386.
- (35) Wu, C. F., Cha, H. J., Rao, G., Valdes, J. J., and Bentley, W. E. (2000) A green fluorescent protein fusion strategy for monitoring the expression, cellular location, and separation of biologically active organophosphorus hydrolase. *Appl. Microbiol. Biotechnol.* 54, 78–83.
- (36) Cha, H. J., Wu, C. F., Valdes, J. J., Rao, G., and Bentley, W. E. (2000) Observations of green fluorescent protein as a fusion partner in genetically engineered Escherichia coli: Monitoring protein expression and solubility. *Biotechnol. Bioeng.* 67, 565–574.
- (37) Adams, S. R., Campbell, R. E., Gross, L. A., Martin, B. R., Walkup, G. K., Yao, Y., Llopis, J., and Tsien, R. Y. (2002) New biarsenical ligands and tetracysteine motifs for protein labeling in vitro and in vivo: Synthesis and biological applications. *J. Am. Chem. Soc.* 124, 6063–6076.
- (38) Griffin, B. A., Adams, S. R., and Tsien, R. Y. (1998) Specific covalent labeling of recombinant protein molecules inside live cells. *Science* (80-.). 281, 269–272.
- (39) Enninga, J., Mounier, J., Sansonetti, P., and Nhieu, G. T. V. (2005) Secretion of type III effectors into host cells in real time. *Nat. Methods* 2, 959–965.

- (40) Dyachok, O., Isakov, Y., Sågetorp, J., and Tengholm, A. (2006) Oscillations of cyclic AMP in hormone-stimulated insulin-secreting β -cells. *Nature* 439, 349–352.
- (41) Hoffmann, C., Gaietta, G., Bünemann, M., Adams, S. R., Oberdorff-Maass, S., Behr, B., Vilardaga, J.-P., Tsien, R. Y., Ellisman, M. H., and Lohse, M. J. (2005) A FlAsH-based FRET approach to determine G protein—coupled receptor activation in living cells. *Nat. Methods* 2, 171–176.
- (42) Zürn, A., Klenk, C., Zabel, U., Reiner, S., Lohse, M. J., and Hoffmann, C. (2010) Site-specific, orthogonal labeling of proteins in intact cells with two small biarsenical fluorophores. *Bioconjugate Chem.* 21, 853–859.
- (43) Hoffmann, C., Gaietta, G., Zürn, A., Adams, S. R., Terrillon, S., Ellisman, M. H., Tsien, R. Y., and Lohse, M. J. (2010) Fluorescent labeling of tetracysteine-tagged proteins in intact cells. *Nat. Protoc.* 5, 1666–77.
- (44) Cheng, Q., Ruebling-Jass, K., Zhang, J., Chen, Q., and Croker, K. M. (2012) Use FACS sorting in metabolic engineering of Escherichia coli for increased peptide production. In Microbial Metabolic Engineering. Methods in Molecular Biology (Methods and Protocols) (Cheng, Q., Ed.), pp 177–196, Springer, New York, NY.
- (45) Machleidt, T., Robers, M., and Hanson, G. T. (2006) Protein labeling with FlAsH and ReAsH. *Methods Mol. Biol.* 356, 209–220.
- (46) Zordan, R. E., Beliveau, B. J., Trow, J. A., Craig, N. L., and Cormack, B. P. (2015) Avoiding the ends: Internal epitope tagging of proteins using transposon Tn7. *Genetics* 200, 47–58.
- (47) De Nobel, J. G., and Barnett, J. A. (1991) Passage of molecules through yeast cell walls: A brief essay-review. *Yeast* 7, 313–323.
- (48) Kiseleva, E., Allen, T. D., Rutherford, S. A., Murray, S., Morozova, K., Gardiner, F., Goldberg, M. W., and Drummond, S. P. (2007) A protocol for isolation and visualization of yeast nuclei by scanning electron microscopy (SEM). *Nat. Protoc.* 2, 1943–1953.
- (49) Ovalle, R., Lim, S. T., Holder, B., Jue, C. K., Moore, C. W., and Lipke, P. N. (1998) A spheroplast rate assay for determination of cell wall integrity in yeast. *Yeast 14*, 1159–1166.
- (50) Ovalle, R., Spencer, M., Thiwanont, M., and Lipke, P. N. (1999) The spheroplast lysis assay for yeast in microtiter plate format. *Appl. Environ. Microbiol.* 65, 3325–3327.
- (51) Niu, W., Hart, G. T., and Marcotte, E. M. (2011) High-throughput immunofluorescence microscopy using yeast spheroplast cell-based microarrays. *Methods Mol. Biol.* 706, 83–95.
- (52) Aguilar-Uscanga, B., and François, J. M. (2003) A study of the yeast cell wall composition and structure in response to growth conditions and mode of cultivation. *Lett. Appl. Microbiol.* 37, 268–274.
- (53) Dominguez, R., and Holmes, K. C. (2011) Actin structure and function. *Annu. Rev. Biophys.* 40, 169–86.
- (54) Baschong, W., Suetterlin, R., and Laeng, R. H. (2001) Control of autofluorescence of archival formaldehyde-fixed, paraffin-embedded tissue in confocal laser scanning microscopy (CLSM). *J. Histochem. Cytochem.* 49, 1565–1571.
- (55) Kwak, S., and Jin, Y. S. (2017) Production of fuels and chemicals from xylose by engineered Saccharomyces cerevisiae: A review and perspective. *Microb. Cell Fact.* 16, 82.
- (56) Moysés, D. N., Reis, V. C. B., de Almeida, J. R. M., de Moraes, L. M. P., and Torres, F. A. G. (2016) Xylose fermentation by saccharomyces cerevisiae: Challenges and prospects. *Int. J. Mol. Sci.* 17, 207.
- (57) Gao, M., Ploessl, D., and Shao, Z. (2019) Enhancing the coutilization of biomass-derived mixed sugars by yeasts. *Front. Microbiol.* 9, 3264.
- (58) Futcher, B., and Carbon, J. (1986) Toxic effects of excess cloned centromeres. *Mol. Cell. Biol.* 6, 2213–22.
- (59) Karim, A. S., Curran, K. A., and Alper, H. S. (2013) Characterization of plasmid burden and copy number in *Saccharomyces cerevisiae* for optimization of metabolic engineering applications. *FEMS Yeast Res.* 13, 107–116.

- (60) Ni, H., Laplaza, J. M., and Jeffries, T. W. (2007) Transposon mutagenesis to improve the growth of recombinant Saccharomyces cerevisiae on p-xylose. *Appl. Environ. Microbiol.* 73, 2061–2066.
- (61) Van Vleet, J. H., Jeffries, T. W., and Olsson, L. (2008) Deleting the para-nitrophenyl phosphatase (pNPPase), PHO13, in recombinant Saccharomyces cerevisiae improves growth and ethanol production on d-xylose. *Metab. Eng.* 10, 360–369.
- (62) Pival, S. L., Birner-Gruenberger, R., Krump, C., and Nidetzky, B. (2011) D-Xylulose kinase from Saccharomyces cerevisiae: isolation and characterization of the highly unstable enzyme, recombinantly produced in Escherichia coli. *Protein Expression Purif.* 79, 223–30.
- (63) Kim, S. R., Ha, S. J., Kong, I. I., and Jin, Y. S. (2012) High expression of XYL2 coding for xylitol dehydrogenase is necessary for efficient xylose fermentation by engineered Saccharomyces cerevisiae. *Metab. Eng.* 14, 336–343.
- (64) Eliasson, A., Hofmeyr, J. H. S., Pedler, S., and Hahn-Hägerdal, B. (2001) The xylose reductase/xylitol dehydrogenase/xylulokinase ratio affects product formation in recombinant xylose-utilising Saccharomyces cerevisiae. *Enzyme Microb. Technol.* 29, 288–297.
- (65) Wang, X., Wang, Z., and Da Silva, N. A. (1996) G418 Selection and stability of cloned genes integrated at chromosomal δ sequences of Saccharomyces cerevisiae. *Biotechnol. Bioeng.* 49, 45–51.
- (66) Routledge, S. J., Mikaliunaite, L., Patel, A., Clare, M., Cartwright, S. P., Bawa, Z., Wilks, M. D. B., Low, F., Hardy, D., Rothnie, A. J., and Bill, R. M. (2016) The synthesis of recombinant membrane proteins in yeast for structural studies. *Methods* 95, 26–37.
- (67) O'Malley, M. A., Lazarova, T., Britton, Z. T., and Robinson, A. S. (2007) High-level expression in Saccharomyces cerevisiae enables isolation and spectroscopic characterization of functional human adenosine A2a receptor. *J. Struct. Biol.* 159, 166–78.
- (68) Johannes, T. W., Woodyer, R. D., and Zhao, H. (2005) Directed evolution of a thermostable phosphite dehydrogenase for NAD(P)H regeneration. *Appl. Environ. Microbiol.* 71, 5728–34.
- (69) Bulter, T., Alcalde, M., Sieber, V., Meinhold, P., Schlachtbauer, C., and Arnold, F. H. (2003) Functional expression of a fungal laccase in Saccharomyces cerevisiae by directed evolution. *Appl. Environ. Microbiol.* 69, 987–95.
- (70) Billi, A. C., Gharaee-Kermani, M., Fullmer, J., Tsoi, L. C., Hill, B. D., Gruszka, D., Ludwig, J., Xing, X., Estadt, S., Wolf, S. J., Rizvi, S. M., Berthier, C. C., Hodgin, J. B., Beamer, M. A., Sarkar, M. K., Liang, Y., Uppala, R., Shao, S., Zeng, C., Harms, P. W., Verhaegen, M. E., Voorhees, J. J., Wen, F., Ward, N. L., Dlugosz, A. A., Kahlenberg, J. M., and Gudjonsson, J. E. (2019) The female-biased factor VGLL3 drives cutaneous and systemic autoimmunity. *JCI Insight 4*, No. e127291.
- (71) Smith, M. R., Bugada, L. F., and Wen, F. (2020) Rapid microsphere-assisted peptide screening (MAPS) of promiscuous MHCII-binding peptides in Zika virus envelope protein. *AIChE J.* 66, No. e16697.
- (72) Jensen, U. B., Owens, D. M., Pedersen, S., and Christensen, R. (2010) Zinc fixation preserves flow cytometry scatter and fluorescence parameters and allows simultaneous analysis of DNA content and synthesis, and intracellular and surface epitopes. *Cytometry, Part A 77A*, 798–804.
- (73) Levitt, D., and King, M. (1987) Methanol fixation permits flow cytometric analysis of immunofluorescent stained intracellular antigens. *J. Immunol. Methods* 96, 233–237.
- (74) Schmittgen, T. D., and Livak, K. J. (2008) Analyzing real-time PCR data by the comparative CT method. *Nat. Protoc.* 3, 1101–1108.
- (75) Eliasson, A., Christensson, C., Wahlbom, C. F., and Hahn-Hagerdal, B. (2000) Anaerobic xylose fermentation by recombinant Saccharomyces cerevisiae carrying XYL1, XYL2, and XKS1 in mineral medium chemostat cultures. *Appl. Environ. Microbiol.* 66, 3381–3386.
- (76) Sekar, R., Shin, H. D., and DiChristina, T. J. (2016) Activation of an otherwise silent xylose metabolic pathway in Shewanella oneidensis. *Appl. Environ. Microbiol.* 82, 3996–4005.
- (77) Shamanna, D. K., and Sanderson, K. E. (1979) Uptake and catabolism of D-xylose in Salmonella typhimurium LT2. *J. Bacteriol.* 139, 64–70.